

## INVESTIGATIONS ON MELTING AND SOLIDIFICATION OF A BATTERY COOLING SYSTEM USING DIFFERENT PHASE CHANGE MATERIALS

by

**Ramu PRADEEP\* and Thangavel VENUGOPAL\***

School of Mechanical and Building Sciences,  
VIT University, Chennai, Tamilnadu, India

Original scientific paper  
<https://doi.org/10.2298/TSCI200229220P>

*The temperature of battery modules in electric vehicles must be controlled adequately to remain within a specified range for optimum performance. In this research work, thermal management of battery modules with PCM was investigated experimentally and computationally. The Li-Ion battery pack cooled with a PCM for removing heat generated during the battery charging and discharging cycles. Computations and experiments were carried out to estimate the heat transfer, solidification and melting characteristics of the PCM used in the thermal management of a Li-Ion cell module. Four PCM (GR44, RT50, OM35, and paraffin wax) with different melting temperature were used for the study. Battery operating temperature and melting point are the key parameters for selection of PCM. Experiments have been carried out only for OM35 and paraffin wax, because OM35 melting point is within the battery operating temperature and paraffin wax for considering harshest condition. The OM35 melting temperature range is below 35 °C which is accordance with a desire to keep battery temperature below that temperature. Based on experimental and simulation results, it was found that OM35 is keeping battery temperature range minimal, which was the ideal for Li-Ion battery thermal management.*

Key words: Li-Ion cell, battery thermal management, PCM, CFD

### Introduction

Transportation has calculable a standout amongst the foremost significant bases of ozone-harming substance, wherever its cause originates from the on-street transportation framework sources. Full battery and plug-in hybrids (BV and PHEV) area unit preserved as hopeful keys to ease surroundings alteration. Electrically powered vehicles aid within the improvement of air quality and reduces the noise in urban regions and facilitate change over to the transportation systems with property energy Park *et al.* [1]. As a result of the big energy and power density of Li-Ion cells, these area unit thought of the prime enabling technology among the battery domain. Several researchers have explored the PCM thermal management system. Single PCM becomes inadequate for higher heat fluxes, like that of wax that has higher heat storage capability however lowers thermal conduction. To determine the balance or trade-off between large heat storage capacity and low thermal conductivity, different methodologies for increasing the conductivity of PCM were inspected. It is also essential to have a uniform

\* Corresponding author, e-mail: [pradeep.r2015@vit.ac.in](mailto:pradeep.r2015@vit.ac.in), [venuengines@gmail.com](mailto:venuengines@gmail.com)

and much stronger battery module to absorb the thermo mechanical effects while it is in operation. It conjointly becomes essential to urge a standardized and far stronger battery module so as to require up the thermo mechanical effects whereas it is operative [2]. The Li-Ion batteries have specific in operation conditions, with the temperature vary being one in all the foremost vital constraints. Optimum in operation temperatures for a Li-Ion cell vary from  $-10$  to  $50$  °C, [3]. The Li-Ion batteries suffering from excessive internal and heat generation and extreme operative temperature eventually fail, probably triggering violent emission and rupture, together with the ignition of active battery material [4]. In any case, by the removal of high current, will increase the heat generation (ohmic  $I^2R$  losses) that results in heating and dropping the life anticipation of the battery pack. Elevated temperatures augment the growth of the solid electrolyte interface layer over time, raising internal resistance and contributing to power loss and capacity fade. Ultimately this leads to a reduction in battery's predetermined life. Though various progressive enhancements are accomplished throughout the year's victimization proceeded with advancement in transferal down within opposition and increasing the heat resilience of its constituents, regardless all vehicles tend to approach bound thermal management. The problems can, in general, be magnified within the battery packs of PHEV wherever the discharge current is relatively high regarding the cell's charge unit capability, that is understood because the C-rate. The C-rates manage charge and discharge rates of A battery. The capability of A battery is going to be often rated at 1 C, which implies that a totally charged battery ought to give 1 A for one hour, rated at 1 Ah, [4]. Notwithstanding considering the total temperature of a battery pack, uneven temperature circulation in a pack ought to be likewise considered. Temperature variety from module to module in a pack could prompt diverse charge/release performance for every module. This, thusly, could prompt electrically irregular modules/packs, and diminished pack performance, [5]. Zhao *et al.* [6] outlined various types of thermal management strategies and got the end that PCM heat dispersal innovation is exceptionally encouraging for battery management frameworks. Karimi *et al.* [7] had an exploratory investigation of a cylindrical shaped Lithium battery thermal management utilizing PCM composites and found that the metal grid PCM composite declines the maximum  $\Delta T$  between battery surface and PCM composite by up to 70%. Wilke *et al.* [8] had a test about preventing thermal runaway propagation Lithium battery packs utilizing a phase change composite material and got that the utilization of stage change composite brings down the maximum temperature experienced by neighboring cells by 60 °C or more. Significant factors harmfully influencing Lithium-particle battery performance is a temperature ascend past rise beyond the normal operating range. Whenever overheated due to short-circuiting or quick charging/releasing procedures the Lithium battery can endure thermal runaway, cell rupture or even explosion, [9]. Novel strategy to think about heat storage performance changes of the framework amid phase change heat storage process and another thought for numerical count of phase change heat storage process, [10]. Review on battery thermal management technologies and thermal safety. The thermal behavior of Li-Ion battery and the adverse effects that high temperature and low temperature imposed on battery performance were focused, [11]. Given a superior knowledge about the warm thermal behavior of cells under various cooling plans by building up a 3-D thermal model for lithium batteries, and to quicken the advancement of the battery thermal management system for vehicle applications, [12]. Melting time and thermal balance temperature of two PCM/3-D-OHP and PCM/OHP systems were studied. The PCM was coupled with two kinds of novel 3-D and 2-D-oscillating heat pipe. Results showed that the paraffin wax/3-D-oscillating heat pipe system needed more time for completely melting of paraffin wax than paraffin wax/oscillating heat pipe system, [13]. Water can be used as an effective thermal energy storage material due

to its higher thermal conductivity excellent freezing/melting characteristics. Freezing and melting experiments were carried out by placing a cylindrical SS capsule filled with nano-composite in a constant temperature bath. The thermal conductivity of pure dionized water was experimentally measured at temperatures ranging from  $-10$  to  $40$  °C. The results showed that the addition of GnP nanoplatelets increased the thermal conductivity of all volume fractions and a maximum of 23.95% enhancement was observed for 0.5% volume fraction in the liquid state, [14]. Cold thermal energy storage for industrial applications such as central air-conditioning in the large buildings, high powered electronic cooling applications, waste heat recovery, food processing, and restoring the electrical power imbalance between daytime need and night-time abundance. Cold thermal energy system incorporating PCM is proved as a viable option for achieving high energy efficiency by many systems. Due to the significance of this issue, many studies have been conducted on the applications of PCM in cold thermal energy storage system. Discusses several factors affecting the thermal conductivity of PCM, such as nanoparticle enhanced PCM, shape of encapsulated PCM, solid volume fraction and particle size, [15]. Investigations have been reported on the degradation in thermophysical properties of a PCM because of repeated thermal cycling. This result indicates the potential of paraffin wax as a heat storage material in latent heat thermal energy storage system, [16]. Peng *et al.* [17] systematically studies the impacts of thermal conductivity and density of PCM on the characteristics of PCM-based thermal energy storage systems. Investigations shows that rapid thermal energy charging/discharging rates, a highly desirable stable working temperature, and orientation-insensitivity of thermal energy storage systems can be achieved using PCM with a high thermal conductivity and a temperature-independent density. Evaluated three different flow parameters of nanofluids and hybrid nanofluids flowing through inside header and riser tube of flat plate solar collector. Maximum dynamic pressure increased in model B for both nanofluid and hybrid nanofluid of about 48% and 16%, respectively. Model B perform better comparing with model A and model C, [18]. A solar thermal water heating system using a custom-built latent heat storage tank with paraffin wax, puretemp 68, and stearic acid/palmitic acid eutectic mixture based PCM was designed, developed and its performance was evaluated in real-time. Domestic hot water system using stearic acid/palmitic acid could be a practical solution for effectively harvesting solar thermal energy for rural areas, [19]. Visual experimental system is built to study the orientations effect on phase change. The melting interface is observed in the experiment. Results demonstrate that the inclination angle has a great influence on the formation and development of natural convection during melting of pure PCM, [20]. Investigated the use of a phase change composite material consisting of paraffin wax and expanded graphite as a potential storage medium for cold thermal energy storage systems to support air conditioning applications. The use of this phase change composite material is novel because of its unique material and thermal characteristics as compared to ice or chilled water that are predominantly used in commercial thermal energy storage systems for air cooling applications, [21]. The applications of PCM in solar energy system, buildings, cooling system, textiles and heat recovery system were analysed and reported, [22].

Most of the aforementioned investigations were conducted under normal battery cell operation, therefore, they cannot provide detailed insights into battery thermal management for scenarios under thermal abuse and possible thermal runaway, which can occur with battery modules in electric vehicles (EV) and hybrid electric vehicles (HEV) when they undergo transient thermal behavior.

The primary goal is to apply the passive cooling system to the EV battery pack using PCM, and the effect of PCM on temperature evaluation and its distribution during high dis-

charge levels in the batteries. In this study different types of PCM with different melting temperature are considered. Hence, during this analysis work, thermal management of batteries with PCM are inspected computationally and through an experiment. The specific objectives of the research are, to evaluate, select appropriate PCM for thermal energy storage, simulate transient temperature distributions in a 3-D finite volume model, to locate hot spots in the sub-module and also evaluate the integrated PCM approach for temperature reduction and uniformity. This research can further be extended to environmental control applications like air conditioning, solar heat pumps and heat recovery in PCM based building services application.

### Physical model

A typical battery contains of an oblong Lithium particle battery (3.8 V, 10 Ah) which is able to operate because the power supply and natural action material are going to be the cooling module, severally. The paraffin is joined to the proper surface of the battery to cut back the contact thermal resistance. The battery pack was thermally shielded from all sides the Lithium-particle battery comprising of a negative current gatherer, negative anode, separator, positive terminal, and positive current authority utilized as an influence supply. The Li-Mn compound (LiyMn) and graphite, severally square measure the active materials of the porous positive and negative electrodes. The chemistry reactions for two electrodes may be written as:

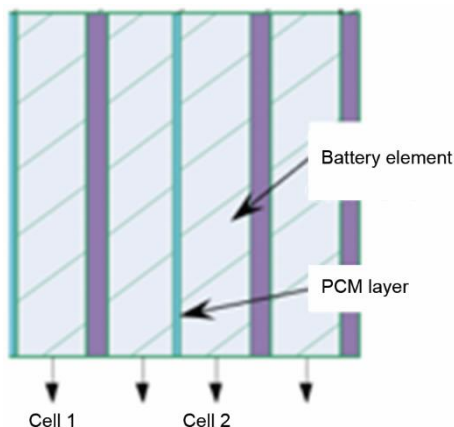
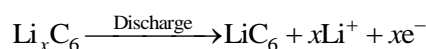
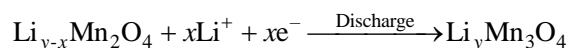


Figure 1. Schematic sketch of the Li-Ion battery with PCM layers

be used with acceptable boundary conditions within the problem solver. The conductor dimensions are 100 mm × 300 mm × 5 mm severally within the breadth  $x$ -height  $x$ -thickness directions.

### Computational investigations

To understand the careful melting and solidifying behavior of the PCM material within the chosen battery system 3-D, incompressible, unsteady state, process fluid dynamic investigations were carried out in commercially offered flow simulation tool, ANSYS FLU-

When the battery is discharged, the PCM absorbs the heat generated from the chemical process happening within the battery. Figure 1 show the schematic sketch of the physical model being studied presently.

### Computational domain

Figure 2 shows the computational model utilized in this study. It consists of a copper plate that is taken into account to get heat, imitating the Li-Ion cell. The heat is taken into account to be generated by victimization the volumetrically heat generation of the copper plate, with the assistance of electrical power provides. The fluid domain of PCM and the solid volume of the copper plate are mainly considered. The walls of the PCM and also the plate was treated absolutely insulated. This can

ENT 15.0, which being a finite volume technique (FVM), based solver. Modelling of the battery and PCM system and meshing of the process domain was carried out using pre-processing tool Gambit 2.4.2 completely different PCM materials paraffin wax and OM35 were chosen for the current study.

### Governing equations

Based on the geometrical dimensions and also the physics concerned – hardening and melting, the Reynolds numbers are calculable to be turbulent at the pipe water. The basic governing equations for flow are the continuity and momentum (Navier-Stokes) equations. The equation for conservation of mass, or continuity equation, additional to ANSYS user guide [23] may be written:

$$\frac{\partial \rho}{\partial t} + \rho \frac{\partial u}{\partial x} + \rho \frac{\partial v}{\partial y} + \rho \frac{\partial w}{\partial z} = 0 \quad (1)$$

For the presently studied case of steady, incompressible flow, the continuity equation can get changed:

$$\frac{\partial u}{\partial x} + \frac{\partial v}{\partial y} + \frac{\partial w}{\partial z} = 0 \quad (2)$$

The equation for the conservation of momentum in a mechanical phenomenon frame of reference is:

$$\frac{\partial(\rho \vec{v})}{\partial t} + \nabla(\rho \vec{v} \vec{v}) = -\nabla p + \nabla(\bar{\bar{\tau}}) + \rho \vec{g} + \vec{F} \quad (3)$$

The equation for the conservation of energy:

$$\rho \frac{\partial H}{\partial t} = \lambda \left( \frac{\rho^2 H}{\rho x^2} + \frac{\rho^2 H}{\rho y^2} + \frac{\rho^2 H}{\rho z^2} \right) \quad (4)$$

where  $\rho$  [kgm<sup>-3</sup>] is the density,  $H$  [J] – the enthalpy,  $\lambda$  – the thermal conductivity, and  $t$  [°C] – the temperature.

Where  $p$  is that the static pressure,  $\bar{\bar{\tau}}$  specifies the strain tensor, and  $\rho \vec{g}$  and  $\vec{F}$  are the attractive force body force and also the external body forces weight (due to gravity) and electro-magnetic severally. These forces are thought of for this study since the influence of those forces on the flow characteristics are going to be there during this system. The PCM once fusible, it will tend to manoeuvre up because of buoyancy, and thus the gravity body force is significant for this study. The easy theme was used for the pressure-velocity coupling and second order up-winding was chosen for discretisation of the governing equations. The strain tensor,  $\bar{\bar{\tau}}$ , is given by:

$$\bar{\bar{\tau}} = \mu \left[ \left( \nabla \vec{v} + \nabla \vec{v}^T \right) - \frac{2}{3} \nabla \vec{v} I \right] \quad (5)$$

where  $\mu$  is the molecular consistence and  $I$  – the unit tensor and therefore the second term on the right-hand aspect is that the impact of volume dilation.

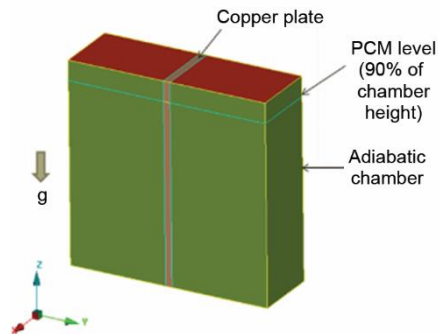


Figure 2. Computational model used in the present study

Percentage of heat transfer coefficient was calculated using conduction equation:

$$Q = -kA \frac{dt}{dx} \quad (6)$$

where  $Q$  [W] is the heat flow through a body per unit time,  $A$  [m<sup>2</sup>] – the surface area of heat flow,  $dt$  [°C] – the temperature difference,  $dx$  [m] – the thickness of body in direction of flow, and  $k$  – the thermal conductivity

### Boundary conditions

Boundary conditions and material properties used for the different combinations of PCM tested presently is shown in tabs. 1 and 2. For any CFD analysis, appropriate boundary condition needs to be specified for an accurate numerical prediction. The boundary conditions used in the present numerical study are summarized in tab. 1. The appropriate values used for the respective boundary surface is tabulated in the last column, as definition. Volumetric heat source was specified for the electrode with 1120000 W/m<sup>3</sup> heat generating capacity. Heat generated by each battery cell is 28 W, which is considered to be the harshest condition, [24]. Honda Insight utilizes a battery pack with six D-sized cells per module, while Toyota Prius battery utilizes further developed prismatic modules of a similar size. The two vehicles utilize 6.5 Ah cells with 6 cells for each module [25]. Based on the volume of the electrode  $5 \times 100 \times 300$  mm<sup>3</sup> appropriate value was specified in the solver. Two-step polynomial functions were used for the properties of the raw PCM and the mixtures studied presently, like thermal conductivity, density, specific heat and viscosity. One value represents the solidified state and the other one represents the liquid state of the PCM. Simulation time is considered 6000 seconds (100 minutes), total number of inner iterations is 10 and total number of time steps 120000. The initial temperature of the entire computational domain was set at 300 K (27 °C). Convergence criteria for the solution from the numerical simulations are considered as converged when all the scaled residuals of the parameters governing the flow such as continuity,  $x$ -,  $y$ -, and  $z$ -momentum are less than or equal to a prescribed value, with computation proceeding unless the prescribed value is reached. The convergence criterion was set as  $10e^{-5}$  for all the governing parameters, in the present computational study. This was maintained for both the validation and present study.

**Table 1. Boundary condition**

Boundary	Description	Definition
Cell boundary	The Li-Ion Cell boundary was considered as adiabatic walls with proper insulation	$q = 0$ W/m <sup>2</sup>
Copper plate	The volumetric heat source is specified for the plate simulating the heat generation during charging and discharging cycles	1120000 W/m <sup>3</sup> [24]

### The PCM used

The OM35, paraffin wax (PALSKEM) and GR44 and RT 50 (Rubitherm GmbH) that's chosen to be used in these analyses comprise of for the foremost half open chain hydrocarbons. The OM35, paraffin wax, GR44 and RT50 are non-dangerous, synthetically latent with most materials and do not represent a risk to either health or the atmosphere. The material properties of all four PCM are presented in tab. 2. It is so indicated within the manufacturer's knowledge that the PCM employed in experiments ought to essentially exhibit stable

characteristics even through perennial activity cycles. During this analysis, there have been several repetitive activity cycles, and no deterioration of the PCM was determined.

**Table 2. Material properties**

Properties	OM35	Paraffin wax	GR44	RT50
Melting temperature [°C]	35	46-58	38-43	45-51
Density – solid	969	818	710	880
Density – liquid	870	760	670	760
Specific heat [KJkg <sup>-1</sup> K <sup>-1</sup> ]	2.57	2.95	2	2.6
Thermal conductivity – S	0.2	0.24	0.2	0.19
Thermal conductivity – L	0.16	0.23	0.14	0.18

### Temperature quantities

In the PCM, consisting of a copper plate, the measurement of the temperature within the instrumentation is completed exploitation K-kind (nickel-chromium/nickel-alumel) of vacuum bottle couples. The sort K thermometer is that the commonest kind of thermometer. Table 3 records the thermometer areas within the framework. Four thermocouples were placed at four indistinguishable profundities within the PCM to quantify abstraction temperature varieties. Figure 3, shows the temperature measurement locations inside the PCM domain.

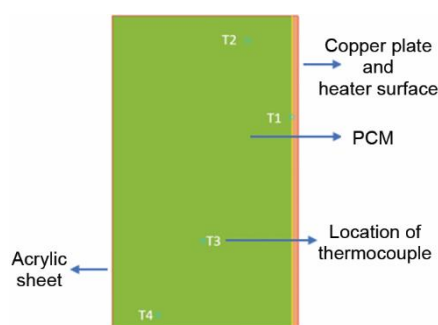


**Figure 3. Temperature measurement locations**

**Table 3. Thermocouple places**

Label	Location	Measures
1	170 mm along y-direction from the base plate of acrylic sheet	Copperplate temperature
2	232 mm along y-direction and 36 mm along x-direction	Inside PCM
3	70 mm along y-direction and 72 mm along x-direction	Inside PCM
4	10 mm along y-direction and 108 mm along x-direction	Inside PCM

### Experimental procedure

#### Preparation of the PCM

The following steps are taken to prepare the PCM material OM35 to battery box:

- Step 1. The thermal chamber temperature is set to 60 °C.
- Step 2. The PCM is kept inside the thermal chamber in a container, where it stays until it melts fully, and the temperature reaches approximately 60 °C.
- Step 3. Molten PCM is poured into the acrylic box according to the volume calculations, box is filled with 90% volume, and remaining 10% of it used for thermal expansion of the material.
- Step 4. The acrylic cover is placed over the box.

Step 5. Acrylic box is placed in the cooling chamber and allow the PCM to solidify.

Step 6. Steps 2 to 5 are repeated for the PCM paraffin wax preparation.

Step 7. Experiments were carried out for the constant heating rate considering the ambient and also with variable heating rates. Dimmer stat used to vary the heating rates and the voltage of-fer to the heater maintained at 120, 160, and 180 V.

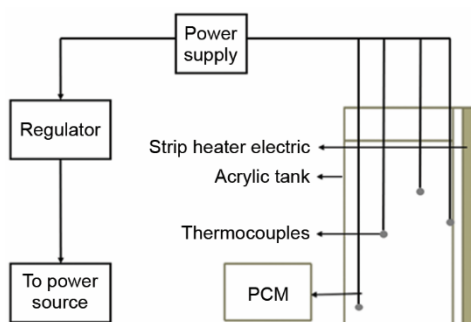


Figure 4. Schematic of experimental set-up

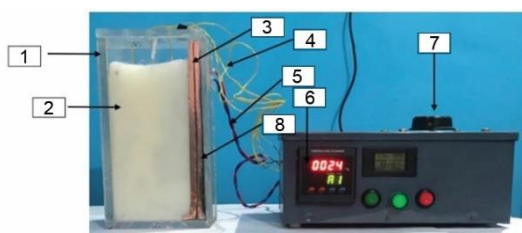


Figure 5. Actual experimental set-up;  
1 – acrylic box, 2 – PCM material, 3 – copper plate,  
4 – thermocouple cables, 5 – power supply cables,  
6 – temperature indicator, 7 – dimmer starter,  
8 – strip heater

process value retransmission output. Dimmer stat had a standard range of 0.75 A, 0-270 V and specifications of no-load current less than 2% of rated capacity testing: as per B.I.S. 5142, tailor made 110V/400 Hz at required current ratings possible. The size of the container used was 300 length mm, 100 mm width, and 300 mm height. The input voltage supply was provided by constant current source from the AC current. During the experiments, the heater surface temperatures, as well as the temperatures at four different locations within the PCM composite, have measured the usage of K-type thermocouples. Thermocouple location,  $T_1$  was selected for temperature of heater surface and  $T_2$ ,  $T_3$ , and  $T_4$  were referred for temperature measurement inside the PCM.

Table 4. Thermocouple range

Type of thermocouple	Temperature range	Standard limits of error	Special limits of error greater
K-type	-200 °C to 1250 °C	2.2 °C or 0.75%	1.1 °C or 0.4%

Figures 4 and 5 show a schematic illustration of the experimental set-up for this study. The instrumentation is formed of acrylic sheet, with a thickness of 12 mm. The length of the instrumentation is 300 mm, the peak of the instrumentation 300 mm, and breadth of the instrumentation is 100 mm. An electrical strip heater through an experiment replicates the battery cell. A copper plate is employed as a bridge between the heater and also the PCM. Since copper may be a sensible conductor of heat and it can give uniform surface distribution. The schematic of the set-up is shown in fig. 4, a constant heat flux battery-like heater or battery simulator was fabricated. The electrical high-powered strip heater (omega strip heater 240 V provide voltage, 150 W power, 10.5 inches length and 2 inches in width) is mounted within the core of a 12 mm thick rectangular acrylic sheet instrumentation. Details of equipment used for the experiments and range K-type thermocouples shown in tab. 4. Strip heater had a maximum operating temperature of 649 °C and wattage tolerances in the range of -10 to 5% at rated voltage. Temperature scanner had 0.1% accuracy and isolated 2X 0/4-20 mA

## Results and discussion

### Melting of PCM paraffin wax, OM35, GR 44, and RT 50 Constant heating rate and ambient temperature

With constant heat generation and ambient temperature, the temperature of a battery increased and reached a steady-state. This specific method was simulated within the experiments and numerically investigated by a relentless heating rate of the heater and thereby exposing it to a stable close temperature.

Figures 6 and 7 show the simulated and experimental results for the paraffin wax and OM35 at location  $T_2$ . These results show that in this experiment, melting of the PCM occurs only on the specified space around the heater, since the temperature at  $T_3$ ,  $T_4$  remain constant no change in temperature was observed.

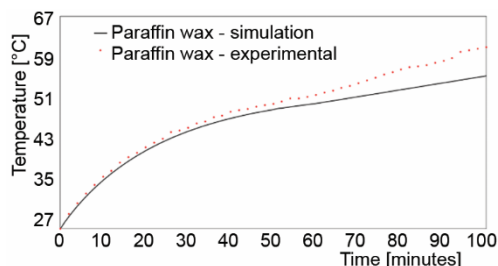


**Figure 6.** Comparison of temperature variation a chosen location in the computational domain and experiment for PCM (paraffin wax) at location  $T_2$

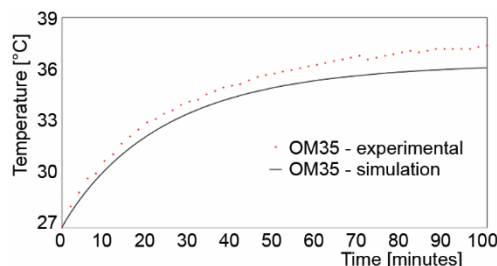


**Figure 7.** Comparison of temperature variation a chosen location in the computational domain and experiment for PCM (OM35) at location  $T_2$

Figure 8 shows the contours of liquid distribution through simulations and fig. 9, shows through experiments. The melting process is controlled by thermal-diffusion consequently temperature contours are associated with the  $x$ -axis. As the buoyancy starts to influence the melting process, thermal coating distribution can be noticed. Vertical temperature gradients are observed in the closeness of the region where the vortex is located. Wherever PCM melting is completed, the energy is stored as sensible heat and it also results in temperature distributions as observed in figs. 8, and 9, for pure paraffin at different time steps of  $t = 0$  minutes,  $t = 30$  minutes,  $t = 60$  minutes, and  $t = 90$  minutes, respectively.

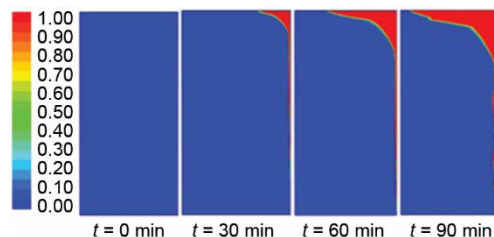


**Figure 8.** Liquid fraction showing the melting pattern of the PCM (paraffin wax) with time

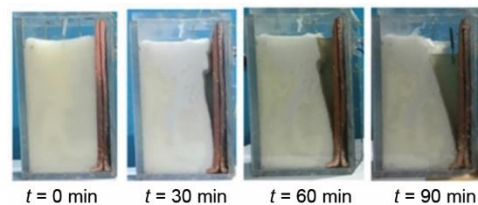


**Figure 9.** Images of melting pattern of the PCM (paraffin wax) with time

Figures 10 and 11 show the temperature of PCM paraffin and OM35 through simulations. Temperature distribution decreased from the battery on the right to the left almost uniformly in PCM zone. At this time, heat dissipation of battery was mainly through heat conduction, because paraffin just began to melt. Temperature distribution of PCM was no longer consistent as the heating time developed gradually. Temperature was higher at the upper right cor-

ner and lower at the lower left corner since the melted PCM, heated by the battery, moved to the upper left region under the effect of buoyancy. The PCM remains the solid phase or mushy phase at the lower right corner and the heat transfer thereof was mainly by heat conduction.

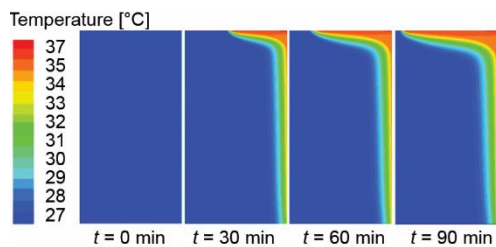


**Figure 10.** Shows the contours of temperature of PCM (OM35) with time

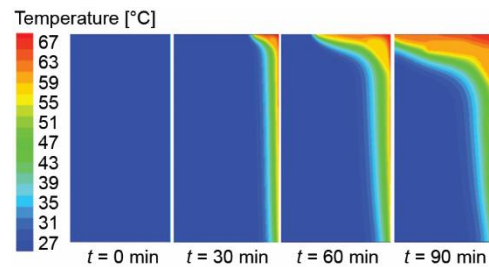


**Figure 11.** Shows the contours of temperature of PCM (paraffin wax) with time

Figures 12 and 13 show the velocity fields for the PCM paraffin and OM35. The flow velocity distribution is funnel shaped, the velocity is slow or even close to zero at the lower right corner. It was clearly observed from numerical and experimental prediction liquid paraffin near the high temperature battery wall flowed upward to the top of the PCM zone due to buoyancy effect and then moved downward along the solid liquid interface that can be seen in velocity fields.

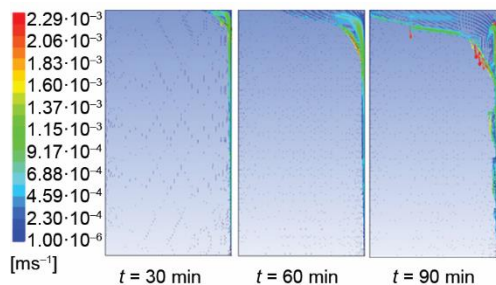


**Figure 12.** Velocity fields for PCM paraffin wax at different time steps

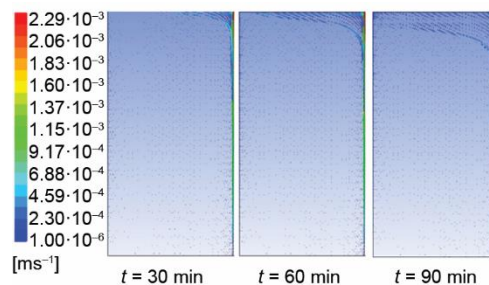
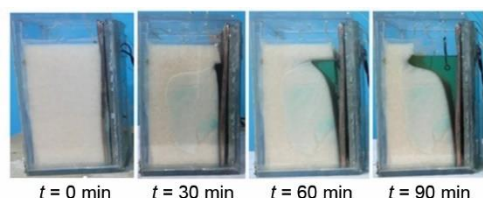


**Figure 13.** Velocity fields for PCM OM35 at different time steps

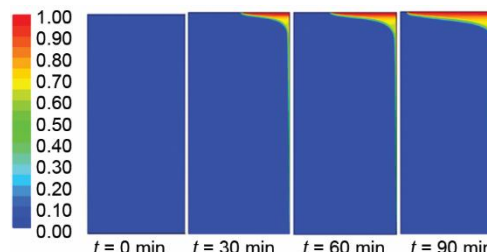
The contours of liquid fraction for the OM35 PCM at different time steps are shown in fig. 14. It was observed that the liquid fraction volume is increasing with time. The liquid zone is increasing in the top zone since hot fluid rises to the top, due to buoyancy. The red color denotes the liquid phase, blue color area was the solid phase and mushy region had a color between the red and blue.

Figure 15 compares the images taken during the experiments in the melting process because of low thermal conductivity of the PCM and the phase change transition from solid to liquid, the temperature rises to the front wall. Convection within the domain is limited by the high viscosity of the initially melted paraffin as the melting proceeds, natural convection becomes increasingly significant.

Figure 16 shows the changes in liquid fraction for PCM material GR 44 as a function of time. As seen in fig. 12 at first, the liquid fraction is zero, however, after a while with heat generation inside the battery the temperatures rise, after the start of discharge the PCM



**Figure 14.** Contours liquid fraction showing the melting pattern of the PCM (OM35) with time



**Figure 15.** Images of melting pattern of the PCM (OM35) with time

starts melting. As time passes the liquid fraction rises and same time the temperature also increased. Figure 17 represents the liquid fraction for the PCM material RT50, the PCM which is direct contact with the heater surface starts melting, despite its longer distance from the battery surface, melting commences earlier. Figure 18 shows the numerical temperature variation results for different types of PCM (paraffin wax, OM35, GR 44, and RT 50) at location  $T_2$ . The OM35 PCM can maintain battery temperature range minimal, which is the ideal for Li-Ion battery thermal management. Reason for selecting the material OM35 considering the operational condition in a vehicle and upper level of temperature that is affects the Li-Ion battery life the melting temperature range is 30 °C to 35 °C which agrees with a desire to keep battery temperatures below 32 °C. The operational conditions and chosen operating range for the PCM warrant some further explanation, as it is commonly held that the Li-Ion battery can safely operate at 45 °C. This is true, however to the extreme detriment in cyclic, and calendar life of the cell. High charge and discharge rates aggravate the impact.

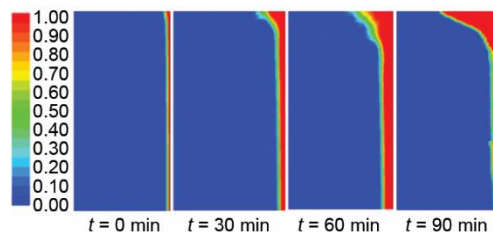


**Figure 16.** Contours liquid fraction showing the melting pattern of the PCM (GR44) with time

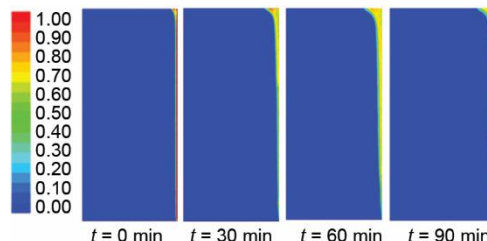


**Figure 17.** Contours liquid fraction showing the melting pattern of the PCM (RT 50) with time

### Temperature distribution and heat loss through PCM and without PCM

The total heat generation quantity in EV or HEV battery pack is depending on the size and design of cooling system. Whereas in Li-Ion battery pack we need to maintain the proper operating temperature and uniform temperature distribution throughout the system. Which is very complex task, in variable ambient conditions.

In order to achieve get higher efficiency and to maintain good operating conditions in the vehicle PCM (OM35 and paraffin wax) materials were used in the experimental studies.

Suitability of the PCM was additionally thought of for variable heating rates of battery cell. For this case, variable heating rates were accomplished with controlled power offer to the electrical heater. As appeared by the broken bend in fig. 19. The voltage offer to the

heater is maintained at 120 W, 160 W, and 180 W. The 160 W with simply air cooling below traditional convection, the heater surface temperature keeps on increasing with higher heating power, demonstrating no pattern of a persistent state. A celestial point temperature of 68 °C was return. Figure 19 demonstrates the heater surface temperature with the same variable heating power.

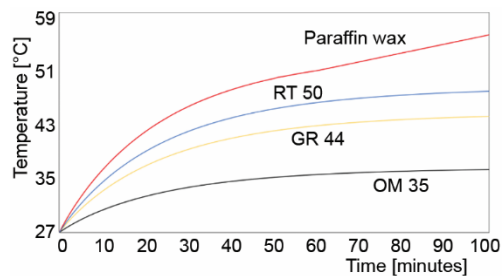


**Figure 18.** Numerical result comparison for different types of PCM at location  $T_2$

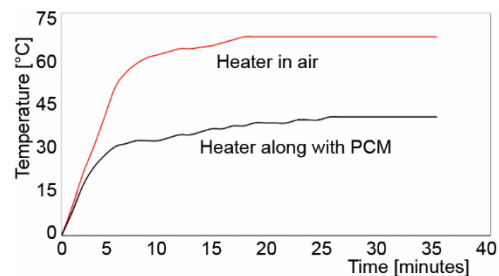


**Figure 19.** Temperature distributions with PCM and without PCM

Figure 19 shows the temperature changes with PCM and without PCM. In simulation we carried out transient implicit steady analysis for 35 minutes of time. Initially, we carried the analysis in ambient condition without using any PCM material. We got the result of 67 °C maximum temperature near the heater cell. In this case the efficiency of system will reduce. Similarly, we used PCM and we got maximum temperature is 35 °C for 35 minutes of time.

## Conclusion

For progressing with the thermal management of EV and HEV, four PCM (GR44, RT50, OM35, and paraffin wax) were used for the study. The present study proposes to include the PCM GR44, RT50, OM35, and paraffin wax with Li-Ion cells. The experimental and numerical results show that PCM absorbed is enough to influence maintaining the best battery temperature powerfully. Thermal management with PCM is investigated in this paper. Careful melting method was studied, and information were reportable. Computations and experiments were dispensed to estimate the heat transfer, melting characteristics of the PCM utilized in the thermal management of a Li-Ion cell module. Four types of PCM were tested computationally and paraffin wax and OM35 were tested experimentally. Computational and experimental results show that OM35 is enough to absorb and maintain the battery temperature. The OM35 is identified as the optimal candidate material as its melting and phase change temperature is coincident with the limiting temperature of the Li-Ion battery. Comparing both OM35 and paraffin wax PCM materials. Paraffin wax, the heat transfer rate was 67% higher compared to OM35 PCM material.

## Nomenclature

$A$  – surface area, [m<sup>2</sup>]  
 $g$  – gravitational acceleration, [ms<sup>-2</sup>]  
 $h$  – heat transfer coefficient, [Wm<sup>-2</sup>K<sup>-1</sup>]  
 $I$  – electric current, [A]  
 $k$  – thermal conductivity, [Wm<sup>-1</sup>K<sup>-1</sup>]

$q$  – heat supplied, [W]  
 $T$  – temperature, [K]  
 $V$  – voltage, [V]

## References

- [1] Park, S., et al., Hybrid Energy Storage Systems and Battery Management for Electric Vehicles, *Proceedings*, 50<sup>th</sup> Annual Design Automation Conference, ACM, Austin, Tex., USA, 2013
- [2] Alrashdan A., et al., Thermo-Mechanical Behaviors of the Expanded Graphite-Phase Change Material Matrix Used for Thermal Management of Li-Ion Battery Packs, *International Journal of Materials Processing Technology*, 210 (2010), 1, pp. 174-179
- [3] Mi, C., et al., Advanced Electro-Thermal Modeling of Lithium-ion Battery System for Hybrid Electric Vehicle Applications, *Proceedings*, IEEE Vehicle Power and Propulsion Conference, Arlington, Tex., USA, 2007, pp. 107-111
- [4] Zhang, X., Multiscale Modeling of Li-Ion Cells: Mechanics, Heat Generation, and Electrochemical Kinetics, Ph. D. thesis, Department of Mechanical Engineering, The University of Michigan, Ann Arbor, Mich., USA, 2009
- [5] Pesaran, A. A., et al., Thermal Performance of EV and HEV Battery Modules and Packs, *Proceedings*, 14<sup>th</sup> International Electric Vehicle Symposium, Orlando, Fla., USA, 1997
- [6] Zhao, J. T., et al., Experimental Study on the Thermal Management Performance of Phase Change Material Coupled with Heat Pipe for Cylindrical Power Battery Pack, *Experimental Thermal and Fluid Science*, 82 (2017), Apr., pp. 182-188
- [7] Karimi., G., et al., Experimental Study of a Cylindrical Lithium Ion Battery Thermal Management Using Phase Change Material Composites, *Journal of Energy Storage*, 8 (2016), Nov., pp. 168-174
- [8] Wilke, S., et al., Preventing Thermal Runaway Propagation in Lithium Ion Battery Packs Using a Phase Change Composite Material: An Experimental Study, *Journal of Power Sources*, 340 (2017), Feb., pp. 51-59
- [9] Linden, D., Reddy, B. T., *Handbook of Batteries*, McGraw-Hill, New York, USA, 2002
- [10] Mao, Q., et al., Energy Storage Performance of a PCM in the Solar Storage Tank, *Journal of Thermal Science*, 28 (2019), 2, pp. 195-203
- [11] Zhoujian, A. N., et al., A Review on Lithium-ion Power Battery Thermal Management Technologies and Thermal Safety, *Journal of Thermal Science*, 26 (2017), 5, pp. 391-412
- [12] Zhuqian, Z., et al., Thermal Modeling and Cooling Analyzis of High-power Lithium Ion Cells, *Journal of Thermal Science*, 20 (2011), 6, pp. 570-575
- [13] Qu, J., et al., Experimental Investigation on the thermal Performance of Phase Change Material Coupled with Three-Dimensional Oscillating Heat Pipe (PCM/3-D-OHP) for Thermal Management Application, *International Journal of Heat and Mass Transfer*, 129 (2019), Feb., pp. 773-782
- [14] Shaji, S., et al., Experimental Investigation of Freezing and Melting Characteristics of Graphene-Based Phase Change Nanocomposite for Cold Thermal Energy Storage Applications, *Applied Sciences*, 9 (2019), 6, 1099
- [15] Sidik, N. A. C., et al., Performance Enhancement of Cold Thermal Energy Storage System Using Nanofluid Phase Change Materials: A Review, *International Communications in Heat and Mass Transfer*, 94 (2018), May, pp. 85-95
- [16] Vasu, A., et al., The Effect of Thermal Cyclic Variation on the Thermophysical Property Degradation of Paraffin as a Phase Changing Energy Storage Material, *Applied Thermal Engineering*, 149 (2019), Feb., pp. 22-33
- [17] Peng, B., et al., Effects of Thermal Conductivity and Density on Phase Change Materials-Based Thermal Energy Storage Systems, *Energy*, 172 (2019), Apr., pp. 580-591
- [18] Farhana, K., et al., CFD Modeling of Different Properties of Nanofluids in Header and Riser Tube of Flat Plate Solar Collector, *Proceedings*, 1<sup>st</sup> Int. Post. Cont. on Mech. Eng., Pehang, Malaysia, Vol. 469, No. 1, 2019
- [19] Prakash, J., et al., Off-Grid Solar Thermal Water Heating System Using Phase-Change Materials: Design, Integration and Real Environment Investigation, *Applied Energy*, 240 (2019), Apr., pp. 73-83
- [20] Yang, X., et al., Effect of Inclination on the Thermal Response of Composite Phase Change Materials for Thermal Energy Storage, *Applied Energy*, 238 (2019), Mar., pp. 22-33
- [21] Aljehani, A., et al., Design and Optimization of a Hybrid Air Conditioning System with Thermal Energy Storage Using Phase Change Composite, *Energy Conversion and Management*, 169 (2018), Aug., pp. 404-418

- [22] Lin, Y., *et al.*, Review on Thermal Conductivity Enhancement, Thermal Properties and Applications of Phase Change Materials in Thermal Energy Storage, *Renewable and sustainable energy reviews*, 82 Part 3 (2018), Feb., pp. 2730-2742
- [23] \*\*\* Ansys Fluent 15.0 Users Guide (2013), SAS IP, Inc
- [24] Dai, H., *et al.*, Design and Simulation of Liquid-cooling Plates for Thermal Management of EV Batteries, *Proceedings*, KINTEX, 2015
- [25] Lukic, S. M., *et al.*, On the Suitability of a New High-Power Lithium Ion Battery for Hybrid Electric Application, *Proceedings*, Future Transport Technology Conference, Costa Mesa, Cal., USA, 2003